Armenian Journal of Physics, 2013, vol. 6, issue 4, pp. 188-197

$Ba_xSr_{1-x}TiO_3$/pc-Si HETEROJUNCTION CAPACITANCE

V. BUNIATYAN[1], C.HUCK[2], A. POGHOSSIAN [2], V. M. AROUTIOUNIAN[3], and M.J. SCHOENING[2]*

[1]State Engineering University of Armenia (SEUA), Yerevan, Armenia

[2] FH Aachen University of Applied Sciences, Institute of Nano- and Biotechnologies, Campus Jülich, Germany

[3] Dept. Phys. Semiconductors and Microelectronics, Yerevan State University (YSU), Armenia

*e-mail: vbuniat@seua.am

Received 18 November 2013

Abstract – An-amorphous $Ba_xSr_{1-x}TiO_3$/ polycrystalline (pc) silicon anis-type heterojunction capacitance was evaluated theoretically and studied experimentally, taking into account the presence of oxygen vacancies in ferroelectric film as well as non-linear dependence of the ferroelectric films dielectric permittivity on the electric field for different values of oxygen vacancies concentration and doping levels in silicon.

1. Introduction

The $Ba_xSr_{1-x}TiO_3$/pc-Si anis-type heterojunction built-in potentials, their distribution across the junction and depletion layers have been examined by us earlier [1]. In this paper, we present systematic calculations of capacitance of $Ba_xSr_{1-x}TiO_3$/pc-Si heterojunction, where the following is taken into account:

a) The dielectric permittivity of ferroelectric films has non-linear dependence on the electric field $\eta(\mathcal{F},r)=\eta(0)(1+A\mathcal{F}^2(x))^{-1}$, where $A=3\ \beta_0\ [\eta_0\eta(0)]^3$, η_0 is the dielectric constant in vacuum ($8.86\cdot10^{-12}$ F/m), $\eta(0)$ is the permittivity at zero bias. For example, for $SrTiO_3$, $\beta_0=8\cdot10^9 Vm^5/C$, $\eta(0)=300$ and $A=0.45\cdot10^{-15}(m/V)^2$ [2];

b) some point defects in ferroelectric materials (for example, inevitably presented oxygen vacancies) create energy levels for charge carriers in the band gap of ferroelectrics, particularly: deep-level trapping states with energies in the range of E_v+2.4 eV to E_v+3.15 eV which lie near the valence band and a series of shallow traps lie near the conduction band edge in the range of $E_C - E_{tn} = 0.06–0.4$ eV. These electron traps are attributed to oxygen vacancies or transition metal/ oxygen vacancy defects [3-9];

c) the high concentration of oxygen vacancy is “endowed” ferroelectric to n-type semiconductor properties and due to the low concentration/non-vacancy, ferroelectric core exhibit p-type properties [3-9];

d) Under applied DC field $\mathcal{F}$, the traps release electron via Pool-Frenkel mechanism and become charged. As a consequence, due to the charge of oxygen vacancies “conditioned” electron levels, the trapped electron occupation (distribution function is changed and new high electric field polarized includes are formed in films). The electric field of a point charge polarizes the crystal locally reducing its permittivity [3, 4, 9].

2. Calculations of BST/pc-Si heterojunction capacitance

It was assumed during consideration of the M-BST/pc-Si-M structure that metal contacts are nearly Holmic (or Schottky) contacts, interface of ferroelectric has p-type conductivity in "core" far away from heterojunction, and at heterojunction surface in contact to crystalline pSi it has n-type conductivity due to high concentration of oxygen vacancies. It is also assumed that donor-like electron trap levels in the band gap of ferroelectric near conduction band are conditioned mainly by oxygen vacancies (other possible defects, such as strain, interstitial atomic (structural) defects do not considered in this paper) and holes trap levels near the top of valence band are conditioned by other acceptor-like defects. Both trap levels are exponentially distributed in band gap of ferroelectric film. Below the activation temperature, T< T_a, oxygen vacancies without external electric field are neutral (occupied by electrons) and cause elastic deformation of the lattice. In the energy diagram trap levels characterized by the concentrations N_{tn} (for electrons) and N_{tp} (for holes) with the characteristic energies E_{tn} and E_{tp}, below the conductive and up to valence bands edges of BST, respectively (Fig.1). Based on results obtained in [3, 5-9] we have adopted the values of E_{c1}–E_{tn}≈0.09–0.6 eV, $N_{tp}\approx 10^{16} \div 10^{19}$cm^{-3} and $E_{tp} \approx E_{v1} + 1.2\ eV$, $N_{tp\approx}(10^{13} \div 10^{14})$ cm^{-3}, for this consideration (Fig.1). It is well known [10-15] that transition between the two materials at the heterojunction interface causes energy discontinuities in the conduction and valence bands, ΔE_c and ΔE_v, in the vicinity of the metallurgical junction. In addition, a dipole layer may appear at the junction and various kinds of imperfections at the interface may result in interface changes.

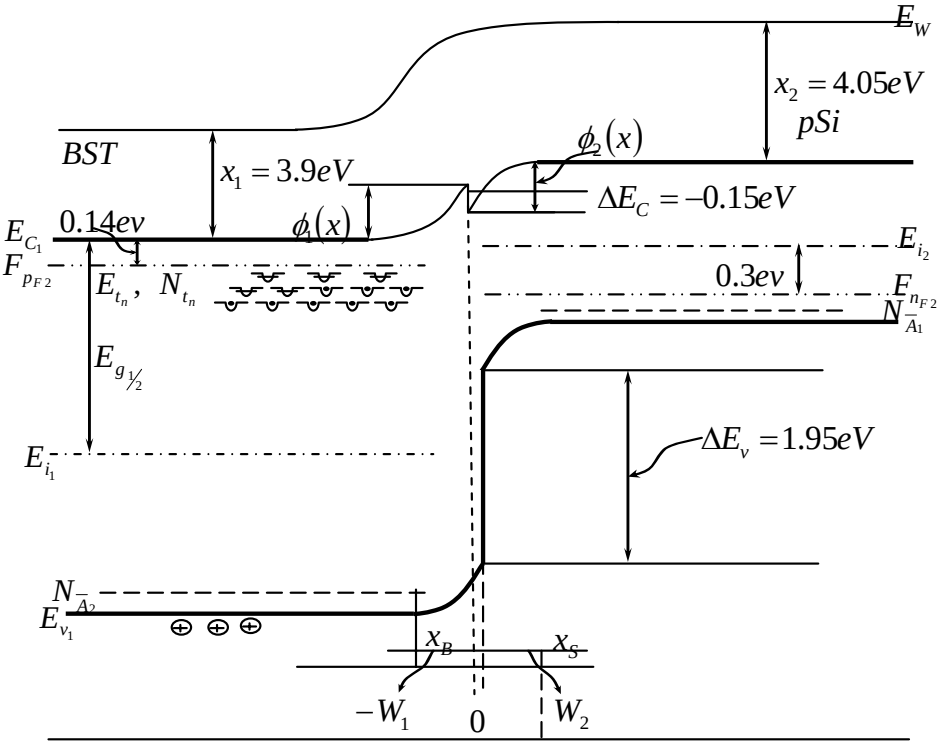

Fig.1. Energy band diagram of the BST/c-pSi heterojunction.

Our calculations have been done for $Ba_{0.25}Sr_{0.75}TiO_3$/c-pSi heterojunction, where Si <100> is doped with B with $\rho \cong 5 \ldots 100\ \Omega cm$, the band gap of BST and Si are 3.2 eV and 1.1 eV, respectively, the electron affinities of

about 3.9 eV and 4.05 eV, respectively. In pc-Si, $\rho \cong 7\Omega cm$ corresponds to the acceptor concentration of N_{A2}^- $\approx 2 \cdot 10^{15} cm^{-3}$ and Fermi quasi level located at 0.31 eV below the mid of forbidden gap (intrinsic Fermi level E_{i2}). Then the work function of p-Si becomes 4.91 eV. Neglecting the free hole concentration in BST in comparison with electrons concentration (oxygen vacancies), we assumed that $N_{tn} \approx 10^{18} cm^{-3}$, the Fermi quasi level for electrons is evaluated 0.14 eV below the conductive band E_{c1}. Thus the work function for BST becomes 4.04 eV ($n_{f1} \approx 10^{17} cm^{-3}$). As it is stated in [16-19], the mismatch of $SrTiO_3$ with Si is ≈1.7% and $BaTiO_3$ is not lattice-matched to Si [15, 17, 19], we have adopted low surface state concentration of about $6 \cdot 10^{10}$ states/cm^2eV. Taking into account above mentioned data, concerning BST / pc-Si, the band structure is constructed based on the Anderson model (Fig.1). The conductance band offset is $\Delta E_c = E_{c2} - E_{c1} - q\Phi_{B0}$ or $\Delta E_c = [x_{BST} - x_{Si}]$ and $\Delta E_c \cong -0.15$eV.The valence band offset is equal to $\Delta E_v = [x_{BST} - x_{Si}] + [E_{gBST} - E_{gsi}]$, therefore $\Delta E_v = 1.95$ eV. As it follows from Fig.2, taking into account that the Fermi level must be constant throughout all system at thermal equilibrium, the built-in potential is equal to $q\Phi_{B0} (= E_{g1}/2 - E_{g2} - \Delta E_c) \cong 0.61\ eV$.

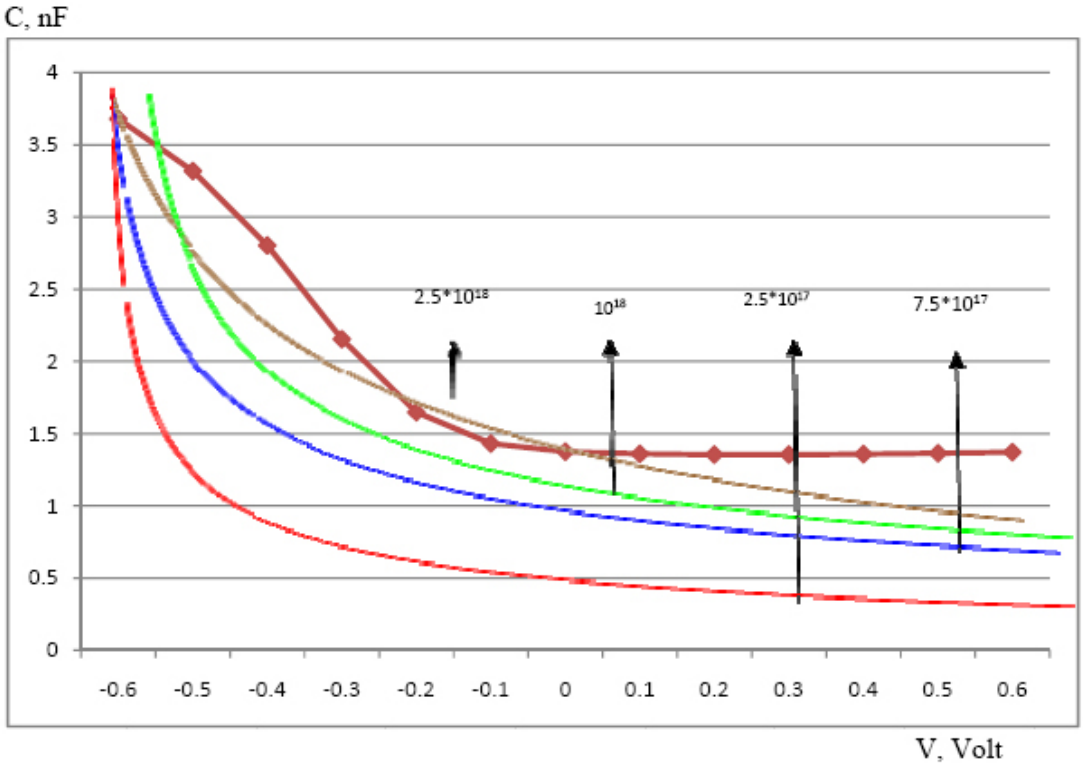

Fig.2. Calculated (-) and measured (exp.), (sample #8892, f=3 kHz, ac V=20 mV) dependences of the heterojunction capacitance C_{het} on voltage, V, for different values of oxygen vacancies concentration, $N_{tn}(cm^{-3})$, (the other parameters are: E_{tn}=0.26 eV, C_{pF}=0.1; Φ_{B0}=0.6 V; η(0)=100; $P_{p0} = 2 \cdot 10^{15} cm^{-3}$; $\sigma_s = 10^{-14}$ cm^2 ; $v_{tn} = 10^7$ cm/s).

We used in this work the depletion approximation and the following mechanism is offered for the establishment of thermal equilibrium condition. As it is assumed high oxygen vacancies in BST interface and $x_{BST} < x_{Si}$, the free electron concentration in BST is larger than that of minority charge carriers (electrons) in p-Si ($n_{po} \approx 10^5 cm^{-3}$, $p_{po} \approx 2.10^{15} cm^{-3}$). After formation of the heterojunction, electrons will be diffused to the pSi conduction band and recombined with holes. BST will be charged positively due to increase in non-compensated oxygen vacancies associated donor-like charges and pc-Si would charge negatively. As ΔE_v is higher and for the

pc-Si holes act as potential barrier, holes cannot diffuse in the BST valence band. Holes from the BST valence band may pass heterojunction and drift to the pc-Si valence band. As BST is charged positively and pSi-negatively, the barrier for electrons will be formed too. We assume that transition from the Si crystalline phase to the BST phase takes place not more than several atomic distances which is rapid enough to be considered an abrupt transition but not so sudden as to give a surface dipole.

As in common cases, the BST/pc-Si heterojunction depletion layer capacitance (for reverse biased) per unit area is defined as C$\equiv \frac{dQ}{d\Phi}$, [15, 20] where dQ is the incremental increase in charge per unit area upon an incremental change of the potential or applied voltage $d\Phi$ (dV). Taking into account the nonlinear dependence of ferroelectric dielectric permittivity on the electric field, we obtain Poisson's equation for the BST depletion layer in the following form [9]:

$$\frac{1-A\mathcal{F}_1^2(x)}{\left(1+A\mathcal{F}_1^2(x)\right)^2}\frac{d\mathcal{F}_1(x)}{dx}=\frac{\rho_1(x)}{\eta_r}, \tag{1}$$

where ρ_1 is the depletion layer charge density of the BST side, $\eta_r=[\eta_0\eta(0)]$.

Using the Gauss's law:

$$Q_s=-\eta_1(\mathcal{F})\mathcal{F}_{10},$$

where $\eta_1(\mathcal{F},r)=\eta(0)(1+A\mathcal{F}^2(x))^{-1}$ is the BST dielectric permittivity, we can calculate the dynamic capacitance of the BST side depletion layer. Integration of Eq. (1)

$$\int_0^{\mathcal{F}_{10}}\frac{(1-A\mathcal{F}_1^2(x))}{[1+A\mathcal{F}_1^2(x)]^2}d\mathcal{F}_1 \quad =\int_{-w_1}^{0}\frac{\rho_1(x)dx}{\eta_r}$$

for the surface maximum electric field $(\mathcal{F})\mathcal{F}_{10}$ [i.e. at x=0 (heterojunction plane) $(\mathcal{F})\mathcal{F}_{10}\,\mathcal{F}(0)=\mathcal{F}_{(\mathcal{F})\mathcal{F}_{10}}$ and $\Phi_1(0)=\Phi_{10}$ gives:

$$\mathcal{F}_{(\mathcal{F})\mathcal{F}_{10}}=\left[\frac{\rho_1(\Phi_{10},x)\Phi_{10}}{\eta_r+A\Phi_{10}\rho_1(\Phi_{10})}\right]^{1/2}.$$

For the BST depletion layer, W'$_1$, dynamic capacitance, $C_{1d,}$ we obtain:

$$C_{1d}\cong\eta_r^2\left(\frac{\rho_1(\Phi_{10},x)}{\Phi_{10}}\right)^{1/2}\frac{\left(1+\frac{\Phi_{10}}{\rho_1(\Phi_{10},x)}\cdot\frac{\partial\rho_1(\Phi_{10},x)}{\partial\Phi_{10}}\right)}{(\eta_r+A\Phi_{10}\rho_1(\Phi_{10},x))^{3/2}}\quad[\tfrac{F}{[cm^2}], \tag{2}$$

where $\rho_1(\Phi_{10},x)=q\{a_1(C_{PF}e^{-\beta\Phi_{10}}-1)+P_{10}(e^{-\beta\Phi_{10}}-1)-n_{10}(e^{\beta\Phi_{10}}-1)\}$, $\beta=q/KT$, $a_1=2N_{tn}B$, $C_{PF}=e^{\beta_{PF}\varepsilon_{10}^{1/2}}$, $B=\frac{\nu\exp(-\beta E_{tn})}{n_{10}S}$, $S=\sigma_s v_{tn}$, σ_s is the capture cross section, $v_{tn}=\left(3KT/m\right)^{1/2}$ is the thermal velocity of electrons, ν is the "attempt to escape" frequency, which is connected to relaxation time with the relationship $\tau=\frac{1}{\nu}\exp(\beta E_{tn})$, and $\beta=q/kT$, q is the electron charge, k is the Boltzmann's constant and T is the absolute temperature.

For the $A\mathcal{F}_{10}^2 \ll 1$ (low field condition that is $(\mathcal{F})\mathcal{F}_{10} \ll 4.71 * 10^5\ V/cm$) case, expression (2) becomes

$$C_{d1} \cong \frac{\eta_r}{\sqrt{2}L_{D1}}.\frac{\left\{\frac{2N_{tn}\beta}{n_{10}}\left(C_{PF}e^{-\beta\Phi_{10}}-1\right)+\frac{p_{10}}{n_{10}}\left(e^{-\beta\Phi_{10}}\right)-\beta\Phi_{10}e+1\right\}}{F_{1s}(n_{10},\Phi_{10},\dots)},$$

where $F_{1s} = \left\{\frac{2N_{tn}\beta}{n_{10}}\left[C_{PF}\left(e^{-\beta\Phi_{10}}(\mathcal{F})\mathcal{F}_{10}-1\right)+\beta\Phi_{10}\right]+\frac{p_{10}}{n_{10}}\left(e^{-\beta\Phi_{10}}-1\right)+e^{\beta\Phi_{10}}-\beta\Phi_{10}-1\right\}^{1/2}$ $L_{D1} = \sqrt{\frac{KT\eta_r}{n_{10}q^2}} = \sqrt{\frac{\eta_r}{q\beta n_{10}}}$ is the extrinsic Debye length for electrons in the BST side.

By the same manner we obtain for the pc-Si side depletion layer per unit area capacitance:

$$C_{d2} = \frac{\eta_2}{\sqrt{2L_{D2}}} =. \frac{\left[1-e^{\beta\Phi_{20}}+\frac{n_{po}}{P_{po}}e^{\beta\Phi_{20}}\right]}{F_{2s}(n_{po},P_{po},\Phi_{20})} \quad \left[\frac{F}{[cm^2]}\right], \tag{3}$$

where $F_{2s}(\Phi_{20}) = \left\{e^{-\beta\Phi_{20}}+\beta\Phi_{20}-1+\frac{n_{po}}{P_{po}}\left(e^{\beta\Phi_{20}}-1\right)\right\}^{1/2}$ and $L_{D2} = \sqrt{\frac{\eta_2}{qP_{po}\beta}}$ is the Debye length for holes in pc-Si and η_2 is the pc-Si dielectric permittivity.

Presented the net depletion layer as W=W$_1$+W$_2$ and $C_{d1,}\ C_{d2}$ as the series connected capacitance and using the relationship $\eta_r\mathcal{F}_{10} = \eta_2\mathcal{F}_{20}$,

e obtain

$$C_{het} = \frac{C_{d1}C_{d2}}{C_{d1}+C_{d2}} = \frac{\eta_r\eta_2\gamma_1\gamma_2}{\eta_r\gamma_1L_{D2}F_{2s}+\eta_2 2L_{D1}F_{1s}},\ \left[\frac{F}{cm^2}\right], \tag{4}$$

where $\gamma_1 = \left[\frac{a_1}{n_{10}}\left(C_{PF}e^{-\beta\Phi_{10}}-1\right)+\frac{P_{10}}{n_{10}}\left(e^{-\beta\Phi_{10}}\right)-e^{\beta\Phi_{10}}+1\right]$, $\gamma_2 = \left[1-e^{-\beta\Phi_{20}}+\frac{n_{po}}{P_{po}}e^{\beta\Phi_{20}}\right]$.

Substituting the expressions for $\gamma_1, \gamma_{2,}$ into expression (4) for C$_{het}$ we obtain

$$C_{het} \cong \frac{\left(q\beta n_{10}P_{po}\eta_2\eta_r\right)^{1/2}\gamma_1\gamma_2}{\left(\eta_r n_{10}\right)^{1/2}\gamma_1F_{2s}+\left(\eta_2P_{po}\right)^{1/2}F_{1s}}. \tag{5}$$

Using the relationship

$$\frac{\Phi_{20}}{\Phi_{10}} = \frac{\rho_1^2d_1\eta_r}{\rho_2^2d_2\eta_2},$$

Aas well as expressions for F_{1s} and F_{s2}

$$\frac{F_{1s}}{F_{2s}} = \frac{\eta_2L_{D1}}{\eta_rL_{D2}}, \quad \Phi_{10} = \frac{W_1^2}{d_1\eta_r}, \quad \Phi_{20} = \frac{W_2^2}{d_2\eta_2}$$

expression of W [1], for C_{het} we obtain:

$$C_{het} \cong \left(\frac{2P_{po}}{n_{po}}\right)^{\frac{1}{2}}\frac{\left[n_{1o}P_{po}N_{tn}\eta_2\eta_1\alpha_1(1+t)(qN^*)^{\frac{1}{2}}\right]}{\sqrt{2(\Phi_{B0}+V)\eta_2\eta_1[\alpha_1^2\eta_2N_{tn}^3+\eta_rP_{po}^3]}}\left[\frac{F}{cm^2}\right],$$

where $d_1 = \frac{1}{q\beta N_{tn}(1+C_{PF})}$, $d_2 = \frac{2}{qP_{po}}$, $\alpha_1 = 2B\varphi_1(1+C_{PF})t^2$, $t = \sqrt[3]{\frac{h_1}{h_2}}$,

$$h_1 \cong \frac{q^2\beta(P_{po}+n_{po})}{2\eta_2}\ ,\ h_2 = \frac{q^2\beta[(P_{10}+n_{10})+2N_{tn}B]}{\eta_r},\quad \varphi_1 = \frac{(P_{10}+n_{10}+2N_{tn}B)}{n_{10}},$$

$$B = \frac{\nu\exp(-\beta E_{tn})}{n_{10}S}\ ,\ N^* = \frac{\eta_1 P_{p0}+2\eta_2 BN_{tn}(1+C_{PF})t^2}{(1+t^2)}\ ,\ \text{(see [1]).}$$

If we represent C_{het} (per unit area capacitance) as

$$C_{het} = \frac{\eta_{eff}}{W}, \tag{6}$$

where η_{eff} denotes heterojunction depletion layer effective dielectric permittivity, then from Eq.(5) η_{eff} can be evaluated as

$$\eta_{eff} = \left(\frac{2P_{po}}{n_{po}}\right)^{1/2}\frac{[n_{10}P_{po}N_{tn}\eta_2\eta_r\alpha_1(1+t)]}{[\alpha_1^2\eta_2 {N_{tn}}^3+\eta_r {P_{po}}^3]}\ ,\ \left[\frac{F}{cm}\right].$$

Using the condition for charge neutrality and equations for depletion layers [1], the ratio of the voltage supported on both sides of the junction is given by ($V=V_1+V_2$)

$$\frac{\Phi_{10}-V_1}{\Phi_{20}-V_2} = \frac{\eta_1\rho_1(x)}{2\rho_2(x)}\ , \tag{7}$$

where V_1 and V_2 are the voltage drops in BST and pc-Si sides, respectively.
As it is assumed that N_{tn} (therefore the electron concentration in BST conduction band is much larger than in pc-Si side), we obtain for the C_{het}:

$$C_{het} = \frac{\eta_{eff}(qN^*)^{1/2}}{\sqrt{2(\Phi_{\beta 0}-V_2)\eta_2\eta_r}}\ . \tag{8}$$

3. Experimental results and conclusions

As it follows from (5), the heterojunction capacitance depends on both BST and pc-Si sides dielectric permittivities, η_2, η_1, as well as oxygen vacancies concentration (through to $\rho_1(x)$, N_{tn}) and doping density of pc-Si, P_{po}.

Calculations of the BST/pc-Si heterojunction capacitance have been carried out for the following parameters listed in Table 1: E_{tn}=0.026…0.6 eV, C_{pF}=0.1; Φ_{B0}=0.6 V; $\eta(0)$=100…200; $P_{p0}=2\cdot10^{15}$ cm^{-3}; $n_i=4.5\cdot10^{10}$ cm^{-3}, N_{tn}= (10^{15}…..10^{19})cm^{-3}; $\sigma_s = 10^{-14}$ cm^2 ; $v_{tn} = 10^7$ cm/s; V=(- 0.6…+0.6) V. The calculated dependence of the heterojunction capacitance C_{het} on the above mentioned parameters are shown in Figs.2-4. The calculated value of the heterojunction capacitance has been compared with the experimental results (Fig.2), carried out for the Al-p-Si-BST(70:30)-Ag structure using an impedance analyzer (Zahner Elektrik). The area of Ag-paste is equals approximately 0.071 cm^2. As it follows from

the Figures, with the increase in the oxygen vacancies concentration, N_{tn}, the heterojunction capacitance increases (Figs. 2, 3) and with the increase in the energy depth of trap levels, E_{tn}, the heterojunction capacitance decreases (Fig.4).

Table 1. The materials parameters.

	E_{g1}, BST	E_{g2}, pc-Si	ΔE_c, eV	$\Delta E_{v,}$eV
Band gap, eV	3.2	1.1	-0.15	1.95
dielect. permit.	200-300	11.8	-	-
electron affinity, x_{BST}, x_{Si}, eV	3.9	4.05	-	-
work function, eV	4.04	4.91		
Fermi quasi-level $E_{c1}-E_{nF1}$, eV $E_{pF2}-E_{v2}$, eV	0.14	0.31		
Chemical potential $\mu_1(E_{g1}/2-F_{nF1})$, eV $\mu_2(E_{C2}-0.85)$, eV	1.46	1.2		

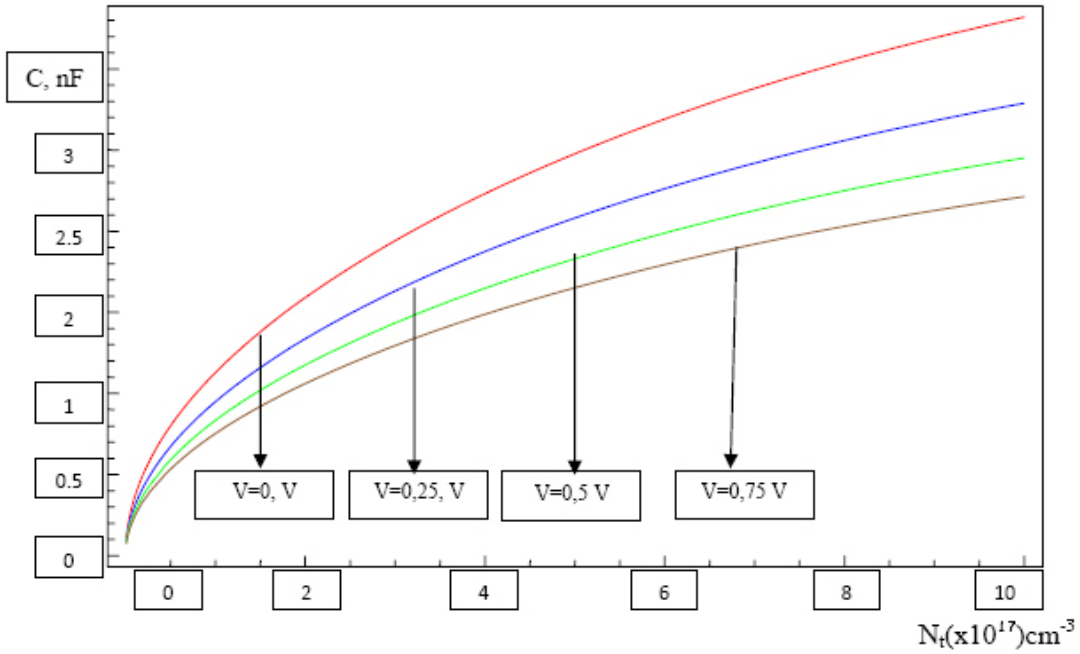

Fig.3. Dependences of heterojunction capacitance C_{het} on oxygen vacancies concentration, $N_{tn}(x10^{17})$, for different values of voltage, V (the other parameters are as in Fig.2.)

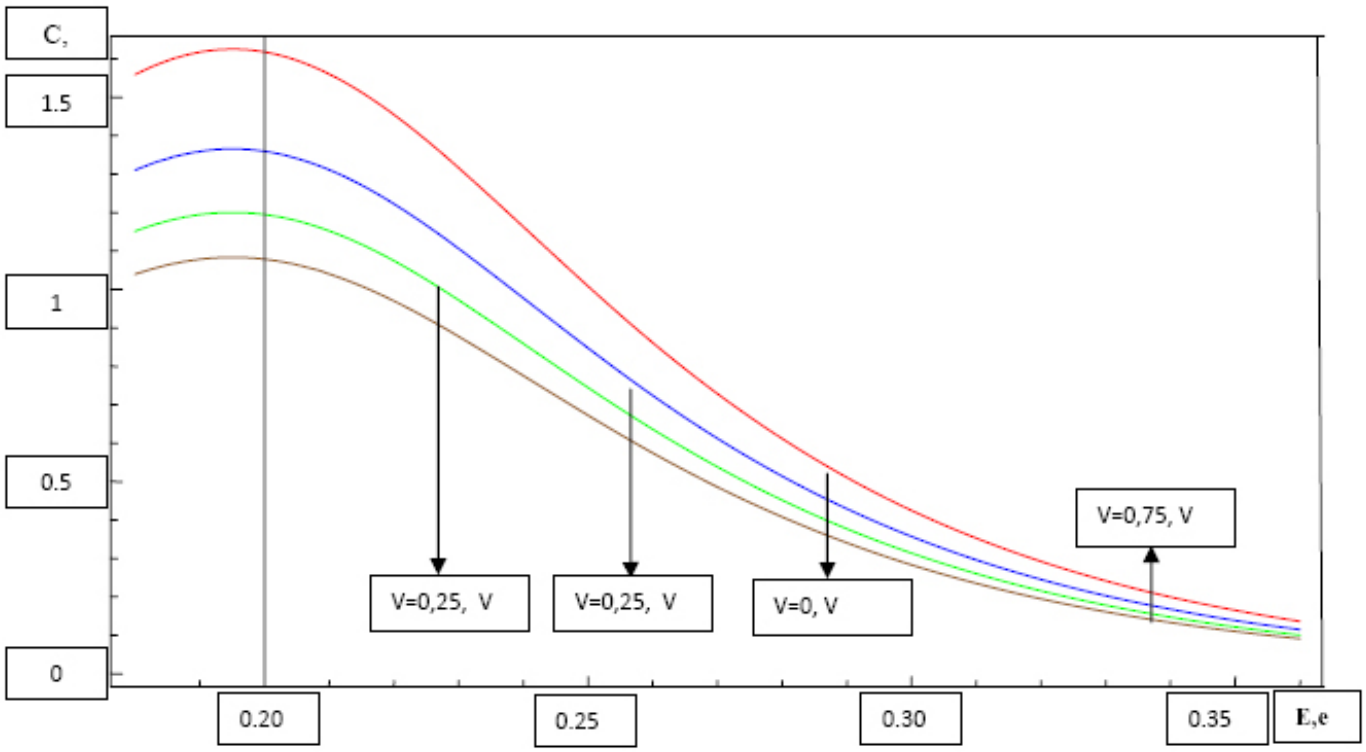

Fig.4. Dependences of the heterojunction capacitance C_{het} on E_{tn} for different values of voltage, V, (other parameters are as in Fig. 2).

From experimental dependence of $C^{-2}(V)$, the built in potential Φ_{B0} has been estimated (Fig.5) which is in the range of theoretical estimation (Φ_{B0} is changed from 0.7 to.0.8 V).

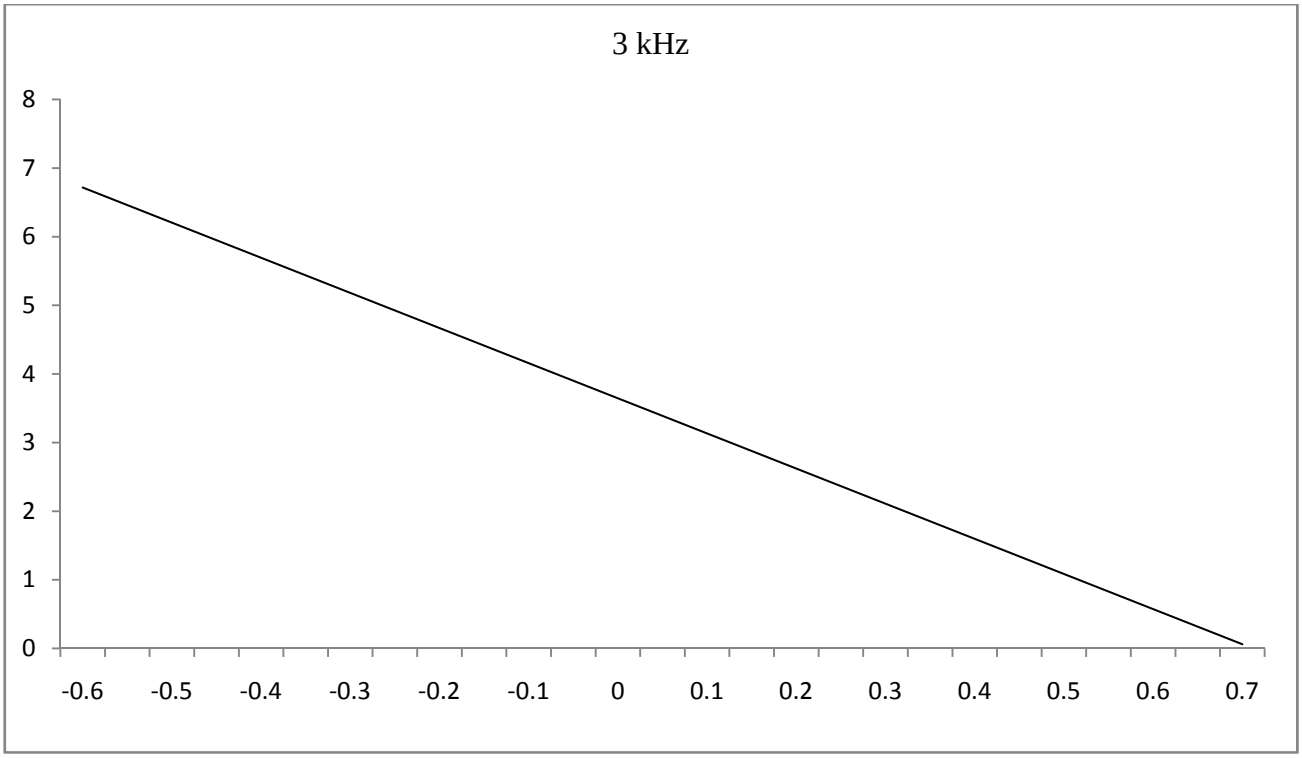

Fig.5.Incremental capacitance characteristic of Al-p-Si-BST(70:30)-Ag heterojunction (area 0.071 cm², $N_{A2}^{-}\approx 2\cdot 10^{15}cm^{-3}$).

Concentration of oxygen vacancies, N_{tn}, has been estimated too, for different energy depths, E_{tn}, of oxygen vacancies conditioned trap levels based on experimental data. For example, from the experiments at V=0 bias voltage C_{het}~1.397 nF (Fig.2). Assume that n_{p0}~$10^5 cm^{-3}$, p_{p0}~$2 \bullet 10^{15} cm^{-3}$, $n_i = 4.5 \bullet 10^{10} cm^{-3}$, $n_{10} = N_{tn} exp\left(-\frac{E_{tn}}{0.026}\right)$, $\eta_{BST}(0)$ ~100, η_{Si}~11.8• $8.85 \bullet 10^{-14} \frac{F}{cm}$, which corresponds to examined structure substrate and measured parameters, from expression (6) one can obtain: N_{tn}~$3.3 \bullet 10^{16} cm^{-3}$ (if E_{tn}=0.26 eV), and N_{tn}~$1.83 \bullet 10^{18} cm^{-3}$(if E_{tn}=0.156 eV). These values of N_{tn} have the same order which is used for theoretical calculations.

From scientific and practical points of view, the research results will contribute to a better understanding of electrochemical, surface and interface properties of perovskite-oxide/silicon films heterojunction exposed to liquid (gas) environments as well as optimizing the sensing characteristics of heterojunction. We anticipate that the new knowledge that emerges from this study will provide the basis for the development of new, combined amperometric/field-effect microsensors for the detection of different biomarkers. The research is directed to develop chemical sensors and biosensors using new materials, new fabrication methods and new sensing principles.

This work was supported by State Committee of Science MES RA, in the frame of the research project *№ SCS 13-2G032.*

R E F E R E N C E S

1. V.V. Buniatyan, C.Huck, A.Poghossian et al. Ba_xSr_{1-x} TiO_3/pc-Si heterojunction built in potential and depletion layer width. J.of Contemporary Physics, Armenian Academy of Sciences, (*in press*)
2. A.K.Tagantsev, V.O. Sherman, K.F. Astafiev et al. Ferroelectric materials for microwave tunable applications, J. Electroceramics., v.11, pp. 5-66, 2003.
3. C.H.Park, D.J. Chadi. Phys. Rev. B57, p.13961, 1998, Microscopic study of oxygen vacancy defect in ferroelectric perovskite, J. Appl. Phys., v.92, N11, pp.6778-6786, Modeling the role of oxygen vacancy on ferroelectric properties.
4. M. Dawber, J. F.Raba, J.F.Scott. Physics of thin film ferroelectric oxides. Rev. of Modern Phys., v.77, pp. 1083-1130, 2005.
5. J.Robertson, Energy levels of point defects in $SrTiO_3$ and related oxides, J. Appl. Phys. v. 93, N2, pp.1054-1059, 2003.
6. J.Robertson. Interfaces and defects of high-K oxides on silicon. Solid State Electronics, v.49, pp.283-293, 2005.
7. A.K. Tagantsev, V.O. Sherman, S. Sh. Gevorgyan, et al. Ferroelectrics in Microwave Devices, Circuits and Systems, Springer, London, 2009, 386p.
8. V.V.Buniatyan, N.W.Martirosyan, A.K.Vorobiev et al. Dielectric model of point charge defects in insulating paraelectric perovskites. J. Appl. Phys., v.110, pp. 09410-1-11, 2010.
9. F. Amy, A.S. Wan, A.Kahn, et al. Band offsets at heterojunctions between $SrTiO_3$, $BaTiO_3$ and Si (100). J. Appl. Phys., 96, 1635, 2007.
10. Z. Luo, J.H. Hao, J. Gao. Rectifying characteristics and transport behavior of $SrTiO_{3-\delta}$ (110)/pSi (100) heterojunctions. Appl. Phys. Lett., v.91, pp.91.062105-1-3, 2007.
11. J. Huang, K. Zhao, H. Lu et al. Characteristics of heterojunctions of amorphous $LaAlO_{2.73}$ on Si. Physica B, 373, 313, 2006.

12. Ch.-l Hu, P. Han, K. Jin et al. Theoretical study of the transport property of p-Si/n $SrTiO_{3-\delta}$. J. App. Phys., v.103, p.103, 053701, 2008.
13. Z. Ling, C. Leach, R. Fzeer. Heterojunction gas sensors for environmental NO_2 and CO_2 monitoring, J. of European Ceram. Society, v.21, pp.1977-1980, 2001.
14. K.F. Brennan, A.S. Brown, Theory of modern electronic semiconductor devices, A Wiley-Interscience Publication, JOHN WILEY & SONS, INC., 2002.
15. C. Jia, J. Chen, J. Guo et al. Valence band offset of InN/$BaTiO_3$ heterojunction measured by X-ray photoelectron spectroscopy. Nanoscale Resarch Letters, v.6, pp.316-1-5, 2011.
16. S.A.Chambers, Y.Liang, Z.Yu et al. Band discontinuities at epitaxial SrTiO3/Si (001) heterojunctions. Appl. Phys., Letters, v.77, p.1662 (2000)
17. C.J. Forst, C.R. Ashman, K. Schwarz et al. The interface between silicon and a high-k oxide. Nature, v.427, N1, pp.53-56, 2004.
18. P.W. Peacock and J. Robertson. Band offsets and Schottky barrier heights of high dielectric constant oxides. J. Appl. Phys., v.92, pp.4712-4721, 2002.
19. S.M.Sze Physics of Semiconductor Devices, 3rd Ed., Wiley Interscience, 2006.